Available online at www.sciencedirect.com
ScienceDirect
Journal of Photochemistry and Photobiology A: Chemistry 188 (2007) 399–408
Journal of Photochemistry and Photobiology A:Chemistry
www.elsevier.com/locate/jphotochem

IR laser-induced co-decomposition of dimethyl selenide and trisilane: Gas-phase formation of SiSe and chemical vapor deposition of nanostructured H/Si/Se/C polymers

Magna Santos [a,*], Luis Díaz [a], Markéta Urbanová [b], Zdeněk Bastl [c], Jan Šubrt [d], Josef Pola [b]

[a] *Instituto de Estructura de la Materia, C.S.I.C., 28006 Madrid, Spain*
[b] *Laboratory of Laser Chemistry, Institute of Chemical Process Fundamentals, A.S.C.R., 16502 Prague, Czech Republic*
[c] *J. Heyrovský Institute of Physical Chemistry, A.S.C.R., 18223 Prague, Czech Republic*
[d] *Institute of Inorganic Chemistry, A.S.C.R., 25068 Řež, Czech Republic*

Received 2 November 2006; received in revised form 15 December 2006; accepted 2 January 2007
Available online 8 January 2007

Abstract

Chemical changes in IR laser irradiated gaseous mixtures of dimethyl selenide and trisilane have been diagnosed by laser-induced fluorescence (LIF) of transient species and by FTIR, Raman, photoelectron spectroscopy and electron microscopy of the final solid products deposited from the gas phase. It is revealed that decomposition of both compounds leads to gas-phase formation of SiSe and deposition of solid nanostructured polymeric materials. We present indirect evidence on the presence of Si—Se bonds in these polymers by revealing that these polymers undergo hydrolysis in air to H_2Se and CH_3SeH, which converts them to solid silicone-based films containing elemental selenium. Plausible reactions taking place in the gas phase and upon exposure of solids to air are suggested.

Keywords: Silicone-based films; Selenium; Laser decomposition; Laser-induced fluorescence; Trisilane; Dimethyl selenide

1. Introduction

The infrared laser-induced photochemistry of gaseous silane has attracted much attention in the past. The IR laser irradiations of silane in a mixture with various compounds have been examined to elucidate chemical steps occurring in the gas phase. The irradiation of silane with sulfur hexafluoride [1] and hexafluorobenzene [2] resulted in explosive reaction and deposition of polymeric materials and that of silane with phosphine, germane, hydrogen chloride, methyl chloride or nitric oxide (all [3]) led to insertion of intermediate silylene ($:SiH_2$) into covalent P–H, Ge–H, C–Cl and H–Cl bonds [3]. Reactions of intermediate silylene have been also deduced to control gas-phase chemistry in mixtures of silane with chlorofluoroethenes [4], trifluoroacetic acid [5], unsaturated esters, aldehydes and ethers (all [6]) in which cases solid silicon-containing (Si/C/F/O or Si/C/H/O) materials have been deposited from the gas phase. These processes allow chemical vapor deposition of solid polymer coatings. IR laser irradiation of silane in mixtures with ammonia or methane has been also examined [7] and shown to yield ultrafine SiC and Si_3N_4 powders. This laser-induced reaction is rather complex and represents an example of the gas-phase formation of simple inorganic compound from two progenitors, each decomposing and providing its element to the reaction product.

Such reactions induced by IR lasers in the gas-phase are, however, rare. We have recently reported that the technique of laser homogeneous pyrolysis (LPHP [8,9]) can be employed to the gas-phase synthesis of nanosized inorganic compounds when clusters of two different elements, simultaneously generated in the gas phase from two progenitors, react in the gas phase. We have shown that the IR laser co-pyrolysis of dimethyl telluride with tetramethyl tin [10] or tetramethylgermane [11] results in chemical vapour deposition (CVD) of nanostructured SnTe or $GeTe_x$ ($x = 1, 2$). (Similar, co-photolytic approach using UV laser irradiation of binary mixtures of tetramethylgermane or tetramethyltin with S precursors (carbon sulfide and thiirane) has been

* Corresponding author. Tel.: +34 91 5616800; fax: +34 91 5645557.
E-mail address: imts406@iem.cfmac.csic.es (M. Santos).

1010-6030/$ – see front matter © 2007 Elsevier B.V. All rights reserved.
doi:10.1016/j.jphotochem.2007.01.001

used by us [12] for chemical vapour deposition of nanostructured tin and germanium sulfides).

Recent years have witnessed an enormous interest in nano-sized particles and nanostructured films of metal chalcogenides (e.g. [13]) including those of 4B group elements (Si, Ge, Sn, Pb, e.g. [14]), whose unique electronic and optical properties are promising for many applications. As for silicon selenides, bulk crystalline and glassy $SiSe_2$ [15] and glassy Si_xSe_{1-x} [16] readily hydrolyze in moist air and SiSe is a rather elusive species produced in the gas phase by discharge and existing only in the gas phase [17] or low-temperature matrix [18]. Nano-sized forms of these materials have not been prepared so far.

In this paper we present an examination of IR laser-induced chemistry in gaseous mixtures of trisilane with dimethyl selenide by laser-induced fluorescence (LIF) spectral monitoring of several transient species and characterize the structure and stability of the solid films deposited from the gas phase. The reported results show transient involvement of SiSe and chemical vapour deposition of nanostructured SiSe-based composites, which are unstable in air and produce nanostructured silicone polymer.

2. Experimental

Gaseous mixtures of trisilane (Si_3H_8) and dimethyl selenide (DMS) were irradiated with pulses from a TEA CO_2 (Plovdiv University, 1300 M model) laser or a Lumonics TEA CO_2 K-103 laser both of which operated at the 10P(26) line of the $00^\circ1 \rightarrow 10^\circ0$ transition at 938.71 cm^{-1}. This wavelength, absorbed by both compounds, was checked in both cases with a 16-A spectrum analyzer (Optical Eng. Co.). The pulses consisted in a spike (60–150 ns (FWHM)) and a tail lasting approximately 1–3 μs.

For the irradiation of the gaseous mixtures and collection of the deposited solid films (KBr or Ta substrates), the output of each CO_2 laser (2.5 J/cm^2 or 65 J/cm^2, 1 Hz) was focused with NaCl lenses (f.l. 15 cm or 10 cm) into two different Pyrex reactors (140 or 95 ml) filled with gaseous Si_3H_8–DMS mixtures (total pressure 27 or 10 mbar) and fitted with NaCl or KBr windows. The reactors were connected to vacuum manifolds through PTFE valves and sample pressures were measured with (0–1 and 0–10 mbar) MKS Baratron gauges.

The progress of the decomposition of both compounds was monitored by gas chromatography (a Shimadzu 14 B chromatograph) and gas chromatography–mass spectroscopy (a Shimadzu QP 5050 mass spectrometer). These analyses employed 25 m long PoraBOND capillary column, programmed (30–160 °C) temperature and sampling by a gas-tight syringe. The chromatograph was equipped with flame-ionization detector and connected with a Shimadzu CR-8A Chromatopac data processor. Decomposition products were identified through their mass and IR spectra using the NIST Chemistry WebBook. For obtaining the IR spectra, FTIR spectrophotometers (Perkin-Elmer 1600 or Nicolet Impact) were used.

For LIF experiments a larger reactor (605 ml) was placed behind a 24 cm focal NaCl lens. The output of a N_2-pumped dye laser (PRA LN107, 0.04 nm bandwidth, 500 ps temporal width), counter-propagating to the pump beam was focused by a 50 cm quartz lens at the focus of the infrared beam. LIF excitation spectra were carried out in different spectral regions by using four different dyes: coumarin 521 (doubled with a KDP crystal) for the 265–272 nm region, stilbene 420 and coumarin 440 for the 412–445 nm region and rhodamine 590 for the 575–600 nm region. The induced fluorescence was collected through a quartz window at the right angle to the laser axis, filtered through a 10 cm-monochromator, 2 mm slit (bandpass of 6.4 nm) at 412–445 nm region and through interference filters centred at 300 and 610 nm at the 265–272 and 575–600 nm regions, respectively. The filtered signal was detected by means of a photo-multiplier (Hamamatsu R-928) fed with 800 or 1000 V.

The CO_2 laser pulse, picked up with a photon drag detector, triggers a Tektronix TDS 540 digital oscilloscope that is used to collect the LIF signals and send them to a personal computer where they are averaged and analyzed. A delay of 10 μs between the CO_2 and probe laser pulses (controlled by a Berkeley Nucleonics digital delay generator BNC 7036A within ∼50 ns) was used for the LIF excitation spectra to avoid spontaneous emission. Each experimental point in a LIF curve was obtained by averaging over ten measurements.

The spontaneous emission spectra were collected at right angle to the laser beam and analyzed with a 0.3 m spectrograph (TMc 300 Bentham) couple to an ICCD detector (2151 Andor Technologies). The spectra were recorded in the range of 220–850 nm with a slit of 1 mm, at zero time delay respect to the irradiation pulse and with an observation window of 5 μs.

The solid films deposited from the gas phase were analyzed by FTIR, Raman and X-ray photoelectron spectroscopy (XPS) and electron microscopy. The FTIR spectra of the films deposited on the KBr substrates were measured directly (*in situ*) in the reactor after evacuation of gaseous products, and after opening the reactor to atmosphere. The gases evolved from the deposited films upon contact to atmosphere were analyzed by the GC/MS technique. The samples on Ta substrates were analyzed by XPS and electron microscopy after exposition to air, or transferred for XPS analysis in the closed reactor filled with Ar.

The Raman spectra of the deposits exposed to air were measured to detect elemental selenium by using a Renishaw RM2000 confocal micro-Raman spectrometer. The excitation source was an Ar^+ laser (514 nm); laser power on the sample was kept under 2 mW to avoid phase transformations. The scattered radiation from the surface was collected in backscattering (180°) geometry at a resolution of 4 cm^{-1}.

The XP spectra were measured using ESCA 310 (Gamma-data Scienta) electron spectrometer. The pressure of residual gases in the analyzer chamber during measurements was in the low 10^{-9} mbar range. The spectra of Si (2p), C (1s), O (1s) and Se (3d) and the spectra of Se $L_3M_{45}M_{45}$ Auger electrons were recorded. The curve fitting of the spectra was accomplished [19] using a Gaussian–Lorentzian line-shape. The decomposition of Se (3d) profiles was made subject to the constraints of the constant $3d_{5/2}$–$3d_{3/2}$ doublet separation (0.9 eV) and the constant intensity ratio ($3d_{5/2}/3d_{3/2} = 1.45$). Quantification of the surface concentrations of elements was accomplished by correcting the photoelectron peak areas for their cross-sections [20].

SEM photographs were obtained using a Philips XL30 CP Scanning Electron Microscope equipped with an energy dispersive analyzer of X-ray radiation Edax DX4. TEM analysis was conducted on a Philips 201 transmission electron microscope at 40 kV on deposited materials scraped the Ta substrate and transferred to a Formvar 1595 E (Merck) membrane-coated Cu grid.

DMS (purity better than 98%) was purchased from Aldrich and trisilane was kindly supplied by Prof. R. Becerra (purity better that 96%).

3. Results and discussion

The irradiation of different mixtures of Si_3H_8 and DMS was accomplished at the 10P(26) line of the CO_2 laser at 938 cm^{-1}, where both molecules absorb. The absorption bands of Si_3H_8 (bending SiH_3 mode [21]) and DMS (CH_3 rocking mode [22]) are consistent with respective molar absorbance of 4.16×10^{-3} and 2.79×10^{-4} cm^{-1} hPa^{-1} at 939 cm^{-1} and allow infrared multiple photon excitation of both compounds.

3.1. Volatile products

The irradiation (0.65–2.5 J/pulse) of different gaseous mixtures of Si_3H_8–DMS results in the decomposition of both compounds and chemical vapor deposition of a yellow-brownish film. The relative depletion of both compounds does not noticeably depend on their initial ratio, which considering by almost one magnitude larger absorbance (ground state optical absorption coefficient) of Si_3H_8, is consistent with a collisionally assisted energy transfer from Si_3H_8 to DMS molecules up to a thermal equilibrium. The IR spectral analysis of irradiated mixtures shows the formation of SiH_4, Si_2H_6, CH_4 and C_2H_2. Their amounts increase with more pronounced depletion of Si_3H_8 and DMS.

The GC–MS and GC analysis of the irradiated mixtures allow a detailed look at the formed volatile products (Fig. 1, Table 1).

The observed volatile products – Si-containing compounds (silane, disilane and methylsilanes $(CH_3)_nSiH_{4-n}$ ($n = 1$–3), hydrocarbons (methane, ethane, ethene and ethyne) and Se-containing compounds (methyl selenide and hydrogen selenide) – are in line with the known mechanisms of the homogeneous decomposition of trisilane and DMS. Si_3H_8 decomposition [23] is controlled by silylenes elimination and insertion reactions leading to formation of silane and Si_nH_{n+2} polysilanes. These initial products undergo [23,24] the same elimination/insertion steps, combination of silylenes and dehydrogenation steps, finally leading to hydrogenated silicon [25]. LPHP of DMS occurs via transient selenoformaldehyde and extrusion of Se, it yields methane, ethane and ethene as three major volatile products and affords chemical vapor deposition of elemental selenium and poly(selenoformaldehyde) [26].

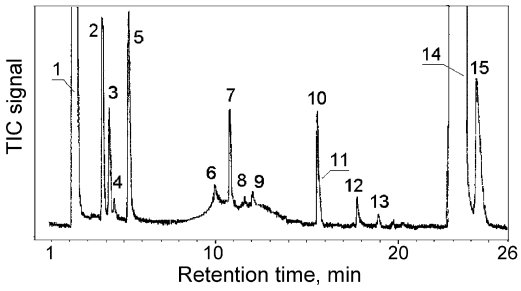

Fig. 1. Typical GC/MS trace of the Si_3H_8–DMS mixture irradiated with 1300 M laser. Peak designation: (1) air + CH_4; (2) SiH_4; (3) C_2H_4; (4) C_2H_2; (5) C_2H_6; (6) H_2Se; (7) CH_3SiH_3; (8) C_3H_6; (9) H_2O; (10) Si_2H_6; (11) $(CH_3)_2SiH_2$; (12) CH_3SeH; (13) $(CH_3)_3SiH$; (14) $(CH_3)_2Se$; (15) Si_3H_8.

The volatile H_2Se, CH_3SeH and $(CH_3)_nSiH_{4-n}$ (Fig. 1) reveal interference of both decompositions: H_2Se and CH_3SeH compounds were not detected in the LPHP of dimethyl selenide [26] but in co-LPHP of 1,3-disilacyclobutane and DMS [27]. They are in line with H-abstraction by Se and $CH_3Se^{\bullet}$ radical from silanes. Methylsilanes $(CH_3)_nSiH_{4-n}$ indicate reaction between $CH_3^{\bullet}$ radical(s) and silylene/and Si-centred radicals. Their yield is estimated to be below 5% and decreases with higher n and less DMS in the initial mixture (Table 1).

The reaction steps involved in the decomposition of Si_3H_8 and DMS as well as those representing interference between the simultaneously decomposing Si_3H_8 and DMS and leading to incorporation of CH_3 group in gaseous and solid (see later) products are schematically presented in Scheme 1. This scheme also includes possible reaction of silylenes with Se_2 and that between Si and Se clusters, both giving SiSe. We point out that the reactions between silylenes and Se_2 get support from the observation of H_2Se and CH_3SeH and from their similarity to reactions of silylene with $^3O_2$ [28].

Table 1
Relative amounts of volatile products at different Si_3H_8/DMS ratios

Irradiated mixture[a], molar Si_3H_8/DMS ratio	No. of pulses	Conversion		Product TIC[b] area/Si_3H_8 decomposed (mole)[c]					$(CH_3)_nSiH_{4-n}/CH_3SiH_3$, GC areas	
		Si_3H_8 (%)	DMS (%)	SiH_4	Si_2H_6	CH_3SiH_3	H_2Se	CH_3SeH	$n = 2$	$n = 3$
0.33	70	28	30	1.8	0.6	0.6	0.04	0.07	0.30	0.10
1.0	40	28	32	0.9	0.5	0.5	0.04	0.09	0.10	0.03
3.0	30	32	38	1.0	0.3	0.1	–	–	c	c

[a] Total pressure 27 mbar; fluence 10 J/cm^2.
[b] Total ion current.
[c] ±10%. Amounts of $(CH_3)_nSiH_{4-n}$ ($n = 1$, 2) under detection limit.

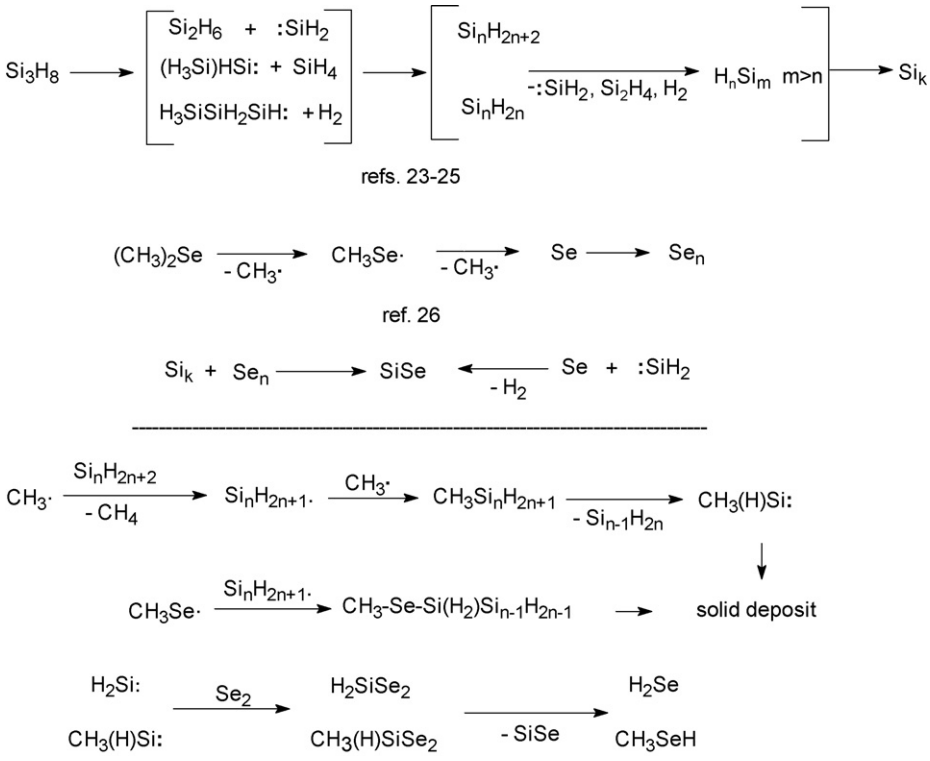

Scheme 1.

3.2. Transient products

An attempt has been made to detect SiSe transient in the gas phase. The formation of Si–Se in UV, 265–270 nm region, can be detected through the $E^1\Sigma^+$–$X^1\Sigma^+$ system [17c], by the transitions $\Delta\nu = 0, -1, -2$. An intense emission signal was observed upon irradiation of the Si_3H_8 + DMS (1:1, total pressure 0.3 mbar) mixture with the IR pulse (0.23 J per pulse) followed by a probe pulse at 265.05 nm. This signal is not seen upon the same irradiation of each separate component. By scanning the probe wavelength a LIF excitation spectrum is obtained given in Fig. 2. Taking into account the values of the spectroscopic vibrational constants given in literature [17c,29], the detected bands are assignable to the sequence $\Delta\nu = 0$ for $\nu = 2$–6 of the $E^1\Sigma^+$–$X^1\Sigma^+$ system of SiSe.

Temporal emission signals were fitted to single exponential decay functions. From the dependence of the inverse decay times against different Ar pressure added to 0.3 mbar of Si_3H_8–DMS mixture, the quenching rate for the $E^1\Sigma^+$ ($\nu' = 3$) state of SiSe by Ar was calculated as $5.84.10^{-11}$ s^{-1} $molecules^{-1}$ cm^3. The extrapolated lifetime for 0 pressure of Ar was 19 ns. This value is in agreement with the radiative lifetime of SiSe as given in the literature [30,31] and is very similar to the corresponding lifetimes calculated at the maxima of the spectrum (Fig. 2) at 264.6, 266.3 and 268.4 nm.

Further LIF experiments were carried out to probe other transients that could be formed in the LPHP of Si_3H_8–DMS mixtures (SiH_2, H_2, Si_n CH_2, and Se_n).

The LIF excitation spectra between 412 and 445 nm of the Si_3H_8–DMS (Fig. 3) show wide bands corresponding to vibrational transitions of Si_2 and Se_2, as well as some much narrower lines corresponding to H_2 (420.2, 421.4, 430.4, 436.3, 440.8, 442.6 nm [32–34] and involving contributions from rotational lines of these species. The assignment of the vibrational bands of the Si_2 and Se_2 in the irradiated Si_3H_8–DMS mixture is based on the LIF excitation spectra of the pure compounds (Table 2) and compatible with the assignments for Si_2 [35] and Se_2 [36]. No other species such as SiH or CH, both of which could have appeared in the same spectral region, have been detected.

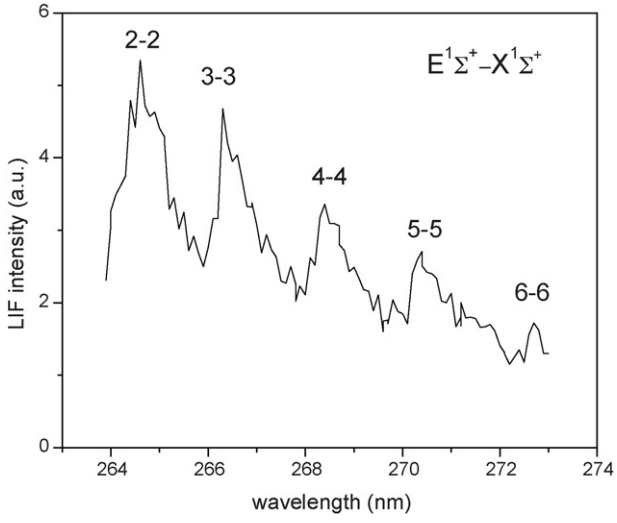

Fig. 2. LIF excitation spectrum from IR decomposition of Si_3H_8–DMS (1:1, total pressure 0.3 mbar).

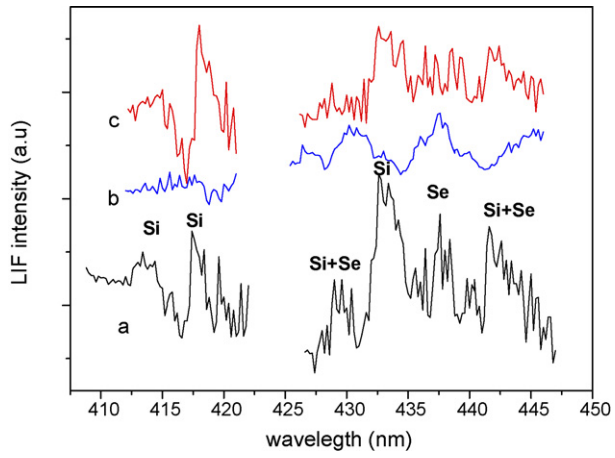

Fig. 3. LIF excitation spectra from IR decomposition of Si_3H_8–DMS ((a) 1:1, total pressure 0.3 mbar); DMS ((b) 0.5 mbar); and Si_3H_8 ((c) 0.3 mbar). The corresponding transitions are given in Table 2.

The lifetimes of the signals corresponding to Si_2 and Se_2 are in the range 85–100 ns and 65–80 ns, respectively. These values are in agreement with the values given in the literature for the respective non-radiative lifetimes, 95–120 ns and 58–86 ns [34,37].

The LIF excitation spectrum of the Si_3H_8 + DMS (1:1) mixture in the region 578–581 nm shows an overlap of large luminescence and LIF signals. The emission spectrum obtained upon subtraction (Fig. 4) is similar to that obtained upon LPHP of 1,3-disilacyclobutane [38] (as well as silacyclopent-3-ene [39] and 2-chloroethenylsilane [40]) and assigned to SiH_2 ($A^1B_1 \leftarrow X^1A_1$, $\Delta v = 2$), CH_2 ($^1B_1(0,16,0) \leftarrow {}^1A_1(0,1,0)$) and H_2 species. The rovibronic level lifetimes in SiH_2 ($A^1B_1(0,2,0)$) vary widely from one level to the next by more than two orders of magnitude; this is due [41,42] to mixing of the electronically excited state with background levels in the $X^1A_1(S_0)$ and $a^3B_1(T_1)$ states. We have obtained signals that fit to two exponentials, one with short lifetime in the range 15–30 ns and the other in the range 400–600 ns. These findings show the known complexity of the thermal decomposition of silanes [23–25] and may reflect early and late silylene formation/decay stages of

Table 2
Assignments of emission bands observed upon irradiation of individual Si_3H_8 and DMS

$\lambda_{excitation}$ (nm)	Δ (nm)[a]	Species	Transition (ν', ν'')	Band
414.8	−0.01	Si_2	(4, 2)	$H^3\Sigma_u^- \leftarrow X^3\Sigma_g^-$
418.0	−0.97	Si_2	(5, 3)	$H^3\Sigma_u^- \leftarrow X^3\Sigma_g^-$
426.7	−0.01	Se_2	(1, 6)	$B1_u \leftarrow X1_g$
428.4	−0.03	Si_2	(3, 3)	$H^3\Sigma_u^- \leftarrow X^3\Sigma_g^-$
430.8	−0.42	Se_2	(0, 6)	$B1_u \leftarrow X1_g$
432.7	−0.02	Si_2	(4, 4)	$H^3\Sigma_u^- \leftarrow X^3\Sigma_g^-$
433.0	−0.60	Se_2	(1, 7)	$B1_u \leftarrow X1_g$
436.0	−0.09	Se_2	(2, 8)	$B1_u \leftarrow X1_g$
437.6	−0.70	Se_2	(0, 7)	$B1_u \leftarrow X1_g$
440.0	+0.76	Se_2	(1, 8)	$B1_u \leftarrow X1_g$
442.0	+0.15	Si_2	(4, 5)	$H^3\Sigma_u^- \leftarrow X^3\Sigma_g^-$
445.2	+0.37	Se_2	(0, 8)	$B1_u \leftarrow X1_g$

[a] Δ means the difference between the measured wavelength in our spectra and the corresponding value calculated with the vibrational constants given in [33].

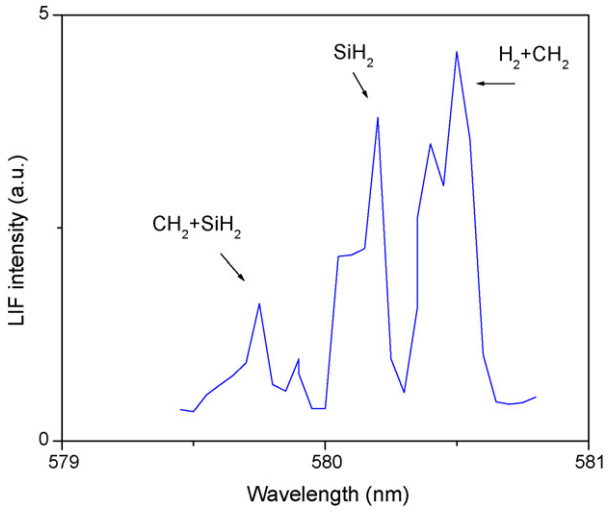

Fig. 4. LIF excitation spectrum from IR decomposition of Si_3H_8–DMS (1:1, total pressure 0.3 mbar), showing contribution of SiH_2, CH_2 and H_2 species. The corresponding transitions are given in the text.

which the former and latter, respectively correspond to primary silylene elimination from Si_3H_8 and silylene eliminations from intermediates.

The time evolution of each of the transients detected in the co-LPHP of Si_3H_8–DMS (1:1) mixture was monitored by means of the curves obtained for each transient by varying the delay between the pump and probe pulses (Fig. 5). The delay of Si_2 and Se_2 has been monitored from the LPHP of pure precursors, while that of SiSe and SiH_2 was followed from the co-LPHP of the Si_3H_8–DMS (1:1) mixture, respectively excited at 266.5 and 580.2 nm. The maxima of these curves are given in Table 3 together with their rise and decay times.

The most intense signals of Se_2, SiSe, SiH_2 and Si_2 occur, in the given order, at 3.5, 1.8, 0.7 and 0.1–0.3 μs after the pump CO_2 laser pulse. The LIF profiles for these three transients can be discussed as follows. The fast formation of the Si_2 and SiH_2 species

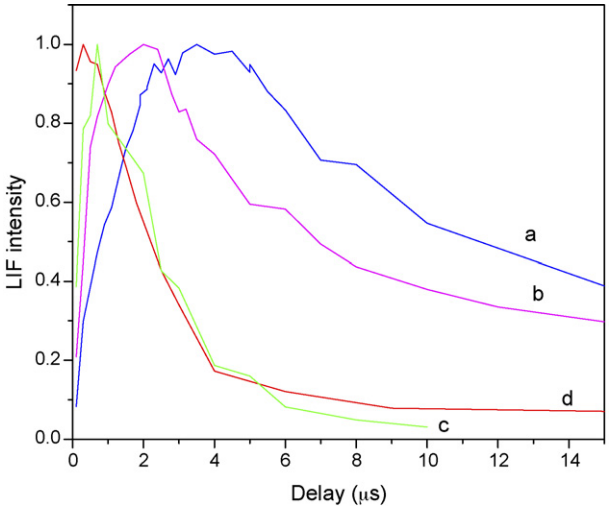

Fig. 5. LIF intensity vs. the delay between the pump and probe pulses for Se_2 from pure DMS (a), for SiSe (b) and SiH_2 (c) from Si_3H_8–DMS mixture, and for Si_2 (d) from pure Si_3H_8.

Table 3
Parameters of delay curves for the different transient species in Fig. 5

Transient	Maximum (μs)	Rise time (ns)	Decay time (μs)
Se_2 (a)	3.5	1800	9.55
SiSe (b)	1.8	600	6.46
SiH_2 (c)	0.7	400	2.30
Si_2 (d)	0.1–0.3	>100	1.50

is in line with silylene elimination and dehydrogenation being the primary channel, while the fast decay of these species must be due to agglomerization reactions. The Si_2 species observed earlier (within the first 100 ns) and depleting faster than SiH_2 is in keeping with its faster agglomerization and/or with the formation of SiSe being faster through the Si_2 + Se than through the SiH_2 + Se channel. The SiSe signal reaches its maximum earlier and decays faster than that of Se_2. This feature is in keeping with a reaction between Si_2 and Se_2 and reflects that some Se_2 species remains unreacted. A simple interpretation of these profiles is not straightforward the above rationale reconciles with the suggested (Scheme 1).

The spontaneous emissions from electronically excited radicals produced in the LPHP process were collected by an ICCD camera. At energies and pressure used in the LIF experiments (0.2 J, 0.3 mbar) only a wide band centred at around 550 nm was found for pure Si_3H_8 and the Si_3H_8 + DMS (1:1) mixture. For higher irradiation energies and pressures, the same band centred at around 550 nm for pure trisilane appears (Fig. 6a), but two new bands are detected in the spectrum of the mixture, one at around 300 nm and the other at 400 nm (Fig. 6b). On the other hand, no spectrum of electronically excited species appears in the irradiation of DMS at any of the used energies or pressures.

The band centred at 550 nm has been assigned [43,44] to emissions from vibrational levels $\nu_2' = 0$–7 of the A^1B_1 electronically excited level of SiH_2 to $\nu_2'' = 0$–4 of the X^1A_1 ground state. The SiH_2 spontaneous emission found in all our conditions has been detected in IR decomposition of several molecules [45,46] as a broad and featureless band in this region. The bands around 300 and 400 nm arise from emissions of different systems of SiSe. Thus, the band at 300 nm can be assigned [47] to transitions $\nu' - \nu''$ ($\nu' = 0$–3, $\nu'' = 0$–6) of the $A^1\Pi$–$X^1\Sigma^+$ system, while the band around 400 nm can be assigned [48] to the progression $0 - \nu''$, $\nu'' = 0$–3 of the spin forbidden transition $a^3\Pi$–$X^1\Sigma^+$. Emissions from the $C^3\Pi \rightarrow X^3\Pi$ system of SiC can [49] contribute also to this last band. These results show that electronically excited SiSe is produced in conditions of irradiation at the higher energies used in this work.

From LIF and spontaneous emission studies it is concluded that SiH_2, CH_2, H_2, Si_2, Se_2 and SiSe transient species in their respective ground states and electronically excited SiH_2 and SiSe are formed in the LPHP of Si_3H_8 + DMS mixtures in agreement with the proposed decomposition Scheme 1.

3.3. Solid products

The FTIR spectra of the *in situ* measured films deposited from Si_3H_8–DMS mixtures (Si_3H_8:DMS = 0.33, 1, 3.0; total pressure 27 mbar) somewhat differ (Fig. 7) from that of the films deposited from neat Si_3H_8. The latter shows [50] composite bands at 625 and 720 cm^{-1} of various H_xSi modes, SiH_2 wagging and scissoring bands at 865 and 899 cm^{-1} and a stretching (SiH_x) band at 2109 cm^1. The former possess additional bands at 1250 cm^{-1} (deformation CH_xM (M = Se [22] and Si) [51]), ~850 cm^{-1} (a blend of stretching Si–C, rocking CH_x and wagging and scissoring modes of SiH_2) and have the Si–H stretching band shifted to higher wavenumbers. This shift is illustrated in the FTIR spectra (wavenumber, cm^{-1} (Si_3H_8/DMS ratio)) of different mixtures – 2123 (3.0), 2132 (1.0) and 2143 (0.33) (Fig. 7) – and is compatible with the presence of H_nSi–Se structures as previously reported [52] for amorphous silicon–selenium alloys. We note that the Si–Se band at 390 cm^{-1} [52] could not be observed under our experimental conditions and that the band for the SiSe reported [18] in the solid argon matrix at 575 cm^{-1} was not observed either.

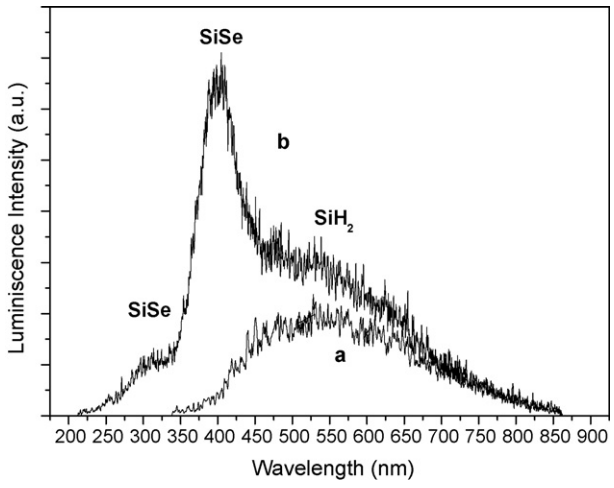

Fig. 6. Spontaneous emission spectra from LPHP of pure Si_3H_8 (a) and of Si_3H_8 + DMS (1:1) mixture (b), both at 1 J and 1–2 mbar. The corresponding transitions are given in the text.

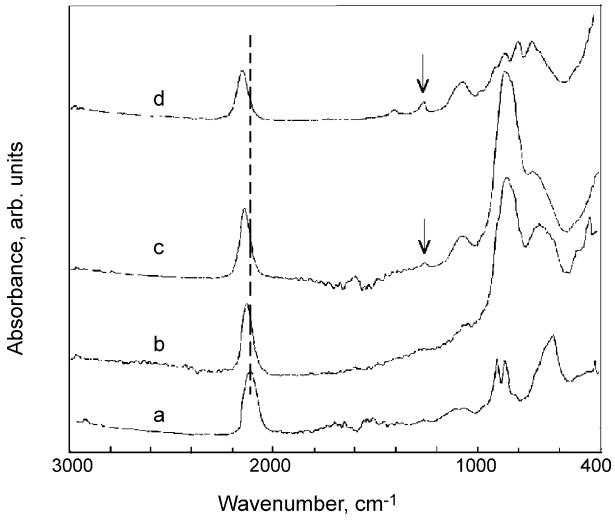

Fig. 7. FTIR absorption spectra of deposited films obtained from Si_3H_8 (13 mbar (a)) and from Si_3H_8–DMS mixtures with Si_3H_8/DMS ratio = 3.0 (b); 1.0 (c) and 0.33 (d); total pressure 27 mbar) (the arrow designates the 1250 cm^{-1} band).

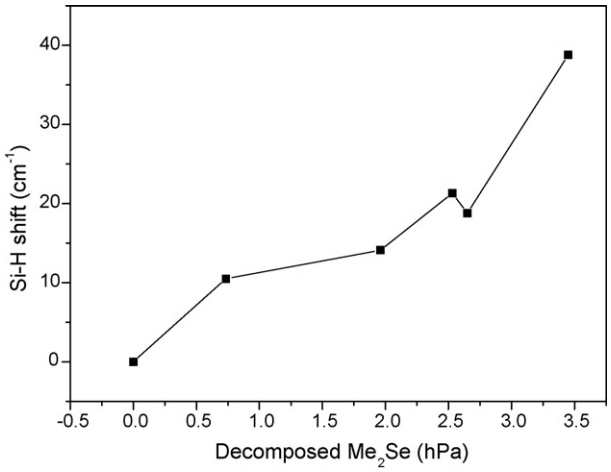

Fig. 8. The shift of the ν(Si—H) band from 2120 cm^{-1} (deposit from pure Si_3H_8) as dependent on the amount of decomposed DMS.

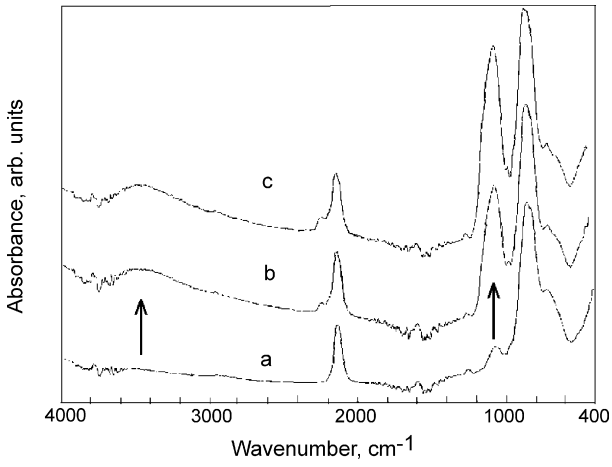

Fig. 9. FTIR spectrum of the deposit from Si_3H_8–DMS mixture (1:1 ratio, 27 mbar) before (a) and after exposure to air for 1 h (b) and 2 days (c) (the arrows indicate the growth of the SiOSi and OHO bands).

The FTIR spectra of the *in situ* measured films deposited from the Si_3H_8–DMS mixtures at total pressure 10 mbar reveal that the Si–H band is detected in the region 2120–2150 cm^{-1} and that the shift to higher wave numbers correlates with the amount of DMS decomposed (Fig. 8). This dependence makes obvious that the formation of the H_nSi–Se bonds becomes more feasible with more DMS decomposition. The absence of the absorption at 575 cm^{-1} (SiSe) suggests that SiSe, proved in the LIF experiments, is highly reactive and decays to yield the H_nSi–Se structures.

The deposits undergo changes upon opening the reactor to air and evolve small amounts of gaseous products. These changes are manifested by FTIR and mass spectra. The films develop new FTIR bands at 1070 and 3480 cm^{-1} (respectively assignable [51] to the SiOSi and O–H . . . O stretching modes) and retain the other bands unchanged (Fig. 9).

The GC/MS analysis of the gases formed upon contact of the films with air were identified [mass spectrum, *m*/*z* (relative intensity in %)] as H_2Se [84 (13), 83 (6), 82 (86), 81 (31), 80 (100), 79 (28), 78 (50), 77 (16), 76 (15)] and CH_3SeH [98 (17), 97 (8), 96 (100), 95 (51), 94 (65), 93 (77), 92 (41), 91 (33), 90 (15), 89 (9), 82 (9), 81 (19), 80 (52), 79 (9), 78 (28), 77 (12) 76 (11)]. These compounds are in line with hydrolysis of Si–Se bonds and provide indirect evidence on the presence of the Si–Se–Si and Si–Se–CH_3 units in the films (Scheme 2). The TIC area of methyl selenide are considerably lower than that of hydrogen selenide (Table 4), which indicates preponderance of the Si–Se–Si units over Si–Se–CH_3 units.

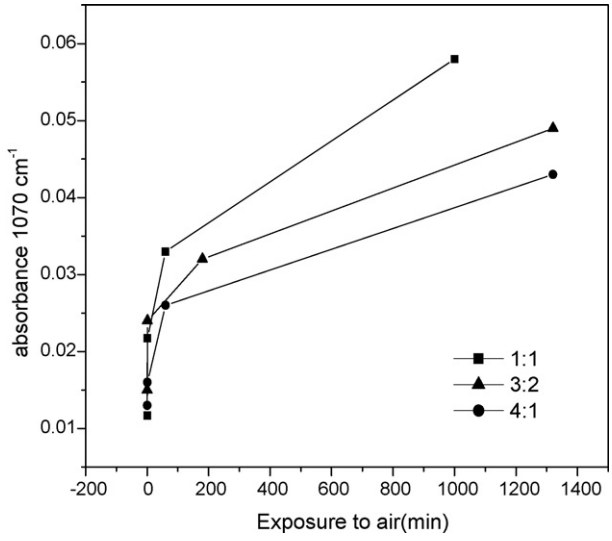

Fig. 10. The growth of the SiOSi absorbance in the films deposited from the Si_3H_8–DMS mixtures (Si_3H_8/DMS ratio 1:1, 3:2 and 4:1; total pressure 10 mbar) exposed to air.

The films deposited from the Si_3H_8:DMS = 1:1, 3:2 and 4:1 and exposed to air build-up the 1070 cm^{-1} band (Fig. 10) at different rate. The hydrolytic process is slower as the proportion of Si_3H_8 in the initial mixture is increased. This may indicate a coating effect of the silicon polymeric film protecting the indirectly proven Si–Se bonds against hydrolysis.

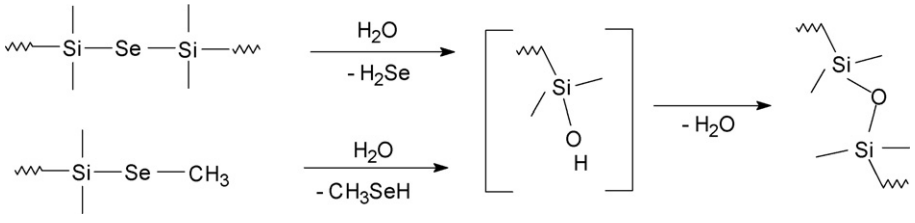

Scheme 2.

Table 4
Analysis of deposited films

Irradiated mixture[a], Si_3H_8/DMS	Decomposed		H_2Se (TIC[b] area)	H_2Se (TIC area)/DMS (decomposed, mbar)	CH_3SeH/H_2Se (TIC area ratio)	Stoichiometry[c]	Contributions of Si units[d]		
	Si_3H_8 (mbar)	DMS (mbar)					$-\underline{Si}C_xH_y-$	C(Si)—$\underline{Si}$—O—	SiO_4
0.33	2.1	6.8	21270	4140	0.02	$Si_{1.00}Se_{0.01}C_{0.30}O_{1.47}$	–	0.20	0.80
1.0	4.4	4.8	6420	1770	0.06	$Si_{1.00}Se_{0.03}C_{0.37}O_{0.84}$	0.23	0.19	0.58
3.0	7.1	2.7	4600	2300	0.01	$Si_{1.00}Se_{0.02}C_{0.19}O_{0.39}$	0.45	0.28	0.27

[a] Total pressure 27 mbar; fluence 10 J/cm^2.
[b] Total Ion Current.
[c] EDX analysis.
[d] As derived from photoemission Si 2p line.

The Raman spectra of the deposited films exposed to air (not given) show bands at 255 and 506 cm^{-1} that are assigned [53] to elemental selenium. Other observed bands at 770 and 1099 cm^{-1} (Si–O bonds [54]) are weak for the films deposited from the mixtures rich in DMS and increase their intensity with the proportion of Si_3H_8. In the deposits obtained from the Si_3H_8-rich mixtures, elemental Se is not observed and c-Si is detected through bands at 517 and 963 cm^{-1}. A band at 388 cm^{-1} related to Si–Se bond [55] is not observed due to hydrolysis of the Si–Se bond in air.

The SEM images of the solid films exposed to air have the same morphology disregarding different conditions of their deposition (Fig. 11). They show fluffy agglomerates with size ranging from ca. 5 to 100 μm. The TEM images show particulate sizes smaller than 30 nm.

The EDX analysis of the films produced from the 27 mbar Si_3H_8–DMS mixtures exposed to air (Table 4) reveals the presence of Si, C, O and Se elements. It shows that the Si content increases, the O content decreases and the C content is not significantly affected with the higher proportion of Si_3H_8 in the initial mixture. The greater incorporation of O is due to hydrolysis of the Si–Se bonds (as reflected with more evolution of H_2Se (and CH_3SeH) in Table 4) and hence with the higher content of the Si–Se bonds in the films prior to exposition to air. The highest efficiency for the Si–Se bond formation is observed at Si_3H_8/DMS = 0.33. The Se observed by the EDX must be in elemental form. The O content being an approximate measure of the Se–Si bonds before exposition to air (a considerably smaller fraction of O may be due to incorporation of O into the Si–C framework [56]), makes us infer that Se is very mostly incorporated in the Si–Se bonds. Ca. 11–17 at% of C in the solid deposits is in keeping with more C incorporation in the solid than in the gaseous products.

The XPS surface stoichiometries, calculated from intensities of photoemission lines, of the films deposited at Si_3H_8/DMS 0.33, 1.00 and 3. 0 at total pressure 27 mbar (in the given order $Si_{1.00}Se_{0.04}C_{0.60}O_{1.69}$, $Si_{1.00}Se_{0.03}C_{0.48}O_{1.22}$ and $Si_{1.00}Se_{0.03}C_{0.31}O_{0.84}$) are in keeping with the EDX—derived composition of the bulk films. The observed values of Se 3d core level binding energies (54.8 eV) and of kinetic energy of corresponding $SeL_3M_{45}M_{45}$ (1G) Auger electrons (1306.4–1306.7) are in accord with elemental selenium [57,58]. Those of Si 2p binding energies (100.0 eV, 102.2 eV and 103.5–104.1 eV) and of Si 2s binding energies (150.3–150.7 eV and 154.2–154.5 eV), respectively indicate [59,60] the presence of $-SiC_xH_y-$, C(Si)–$\underline{Si}$–O– and SiO_4 structural units. The contributions of these units in the films from different Si_3H_8/DMS mixtures differ (Table 4, Fig. 12). The content of SiO_4 unit increases with decreasing Si_3H_8/DMS ratio. Considering that SiO_4 units are generated by hydrolysis of the SiSe and/or $Si(Se-)_x(H)_y$ units in the deposited films upon exposure to air, the highest SiO_4 portion observed for Si_3H_8/DMS = 0.33 confirms (and is in line with above data) that these films possess the most abundant SiSe and/or $Si(Se-)_x(H)_y$ units.

In effort to detect the Si–Se bond, one sample of the film deposited at = 0.33 was transferred to the XP spectrometer immediately after opening the reactor so that the exposure to air was minimized. The surface stoichiometry of this film

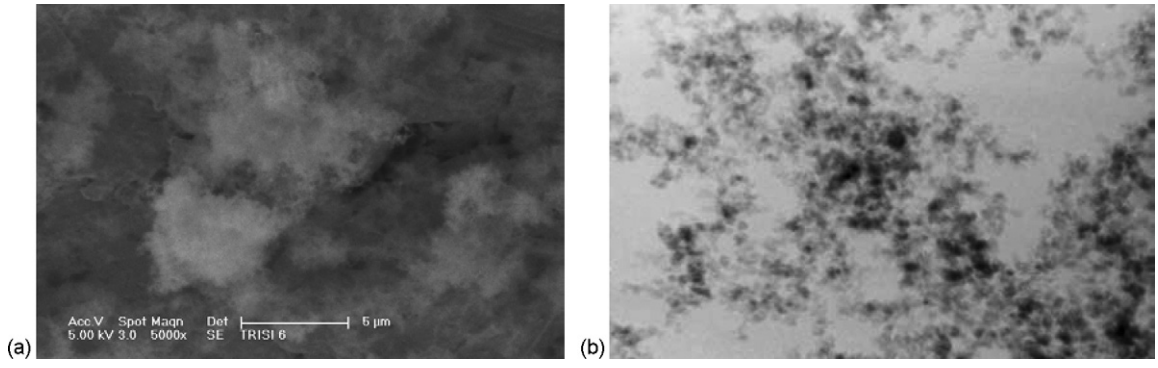

Fig. 11. SEM ((a) 25,000×) and TEM ((b) 100,000×) images of the film deposited from the Si_3H_8–DMS mixture (1:1 ratio, 27 mbar).

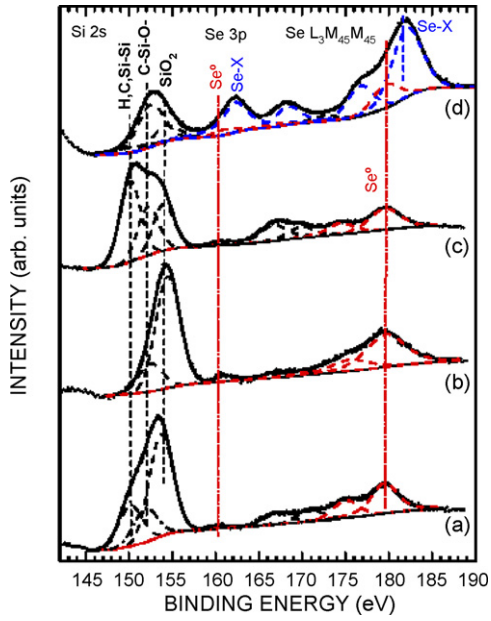

Fig. 12. Spectra of Si 2s, Se 3p and $SeL_3M_{45}M_{45}$ electrons taken from films deposited at Si_3H_8/DMS 1 (a); 0.33 (b); and 3 (c) and compared to those obtained at Si_3H_8/DMS 1 with minimum air exposure (d) (the vertical lines located at 160.5 and 180 eV indicate posicion of Se $3p_{3/2}$ and $SeL_3M_{45}M_{45}$ components belonging to elemental Se).

($Si_{1.00}Se_{0.09}C_{0.38}O_{0.31}$) indicates the higher content of Se and the lower content of O and the XP spectrum (Fig. 12d) reveals different contributions of–SiC_xH_y– (0.13), C(Si)–Si–O– (0.63) and SiO_4 (0.24) structural units; additionally a new signal at 56.2 eV and kinetic energy of corresponding $SeL_3M_{45}M_{45}$ (1G) Auger electrons 1304.6 eV indicate a new form of Se state that can be tentatively assigned to selenium in Si–Se bond

The EDX FTIR, Raman and XPS analysis and behavior of the films in air can be reconciled with LIF detection of SiSe only by assuming that SiSe species is very reactive when produced in the gas phase and that it decays through ensuing reactions to solid products possessing H/C/Si/Se polymeric films.

The SiSe is isovalent to SiO [61,62] that undergoes fast polymerization to structurally inhomogeneous material (e.g. [63–65]). The deposited solids do not show infrared band of SiSe nor (750 cm^{-1} assignable [66], which rules out the possibility of SiSe decay through SiSe polymerization and SiSe decomposition (2 SiSe → $SiSe_2$ + Si [67]). These facts suggest that SiSe gets lost through other sink reactions. The known [68] Si^+–Se^- polarity would favour nucleophilic attack of SiSe to >Si(H)– moieties, leading to the formation of the >Si(H)–Se–Si– structures. Other important reactions can be insertion into Si–H bonds, addition across silene and combination with silylenes, as deduced from analogous steps of isovalent SiO which behaves [69] as a reactive silylene.

4. Conclusions

Infrared laser irradiation of gaseous mixtures of DMS and trisilane results in the formation of transient SiSe, silylene, methylene, Si_2, Se_2 and H_2 species (detected by LIF experiments), the variety of stable volatile products—Si-containing compounds (silane, disilane and methylsilanes $(CH_3)_nSiH_{4-n}$ (n = 1–3), hydrocarbons (methane, ethane, ethene and ethyne) and Se-containing compounds (methyl selenide and hydrogen selenide) and affords chemical deposition of solid nanostructured films containing Si, C, H, Se and O atoms.

Interference of DMS and trisilane decompositions is indicated by the presence of the stable volatile H_2Se, CH_3SeH and $(CH_3)_nSiH_{4-n}$ compounds and by detection of transient signals of SiSe.

The occurrence of SiSe in the solid deposited films is not detected by *in situ* measured FTIR spectra of the films after removal of gaseous products in vacuum.

The films incorporate O and liberate H_2Se and CH_3SeH compounds upon exposure to air. This is in line with the presence of the SiSe and or Si–Se–X (X = Si, C) bonds contained in polysilacarbothienes and with their hydrolysis upon contact to air moisture.

The hydrolysis progress is slower with the films produced from mixtures with higher proportion of trisiliane, which is pointing to some coating effect of the silicon polymeric film protecting the assumed Si–Se bond against hydrolysis.

The absence of gas-phase produced SiSe in the solid phase is judged as caused by its polymerization and/or fast reactions with number of gas-phase produced species.

Acknowledgements

This work has been supported by the Ministry of Education, Youth and Sports (grant ME 846) of the Czech Republic and by Spanish DGI, MCyT (BQU2003-08531-C02-02). We acknowledge the reviewers of J. Photochem. Photobiol. A: Chem. for their valuable comments and suggestions.

References

[1] S.H. Bauer, J.A. Haberman, IEEEJ Quantum Electron. 14 (1985) 233.
[2] Y. Koga, R.M. Serino, R. Chen, P.M. Keehn, J. Phys. Chem. 91 (1987) 298.
[3] (a) F.W. Lampe, Spectrochim. Acta 43A (1987) 257 (and refs. therein); (b) P. Zhu, M. Piserchio, F.W. Lampe, J. Phys. Chem. 89 (1985) 5344.
[4] (a) J. Pola, S. Simeonov, J. Chem. Soc. Perkin 2 (1991) 101; (b) L. Díaz, M. Santos, C.L. Sigüenza, S.A. Simeonov, P.F. González-Díaz, J.A. Garcia Dominguez, R. Fajgar, J. Pola, Z. Bastl, J. Tláskal, J. Chem. Soc. Faraday Trans. 89 (1993) 3907.
[5] J. Pola, Z. Bastl, J. Tláskal, Infrared Phys. 30 (1990) 355.
[6] (a) J. Pola, in: A.R. Basindale, P.P. Gaspar (Eds.), Frontiers of Organosilicon Chemistry, The Royal Society of Chemistry, Cambridge, 1991, p. 159; (b) Z. Papoušková, J. Pola, Z. Bastl, J. Tláskal, J. Macromol. Sci. Chem. A27 (1990) 1015; (c) R. Alexandrescu, J. Morjan, C. Grigoriu, I.N. Michailescu, Z. Bastl, J. Tláskal, R. Mayer, J. Pola, Appl. Phys. 46A (1988) 768.
[7] J.S. Haggerty, W.R. Cannon, in: J. Steinfeld (Ed.), Cannon Laser Induced Chemical Processes, Plenum, New York, 1981.
[8] W.M. Shaub, S.H. Bauer, Int. J. Chem. Kinet. 7 (1975) 509.
[9] D.K. Russell, Chem. Soc. Rev. 19 (1990) 407.
[10] D. Pokorná, J. Boháček, V. Vorlíček, J. Šubrt, Z. Bastl, E.A. Volnina, J. Pola, J. Anal. Appl. Pyrolysis 75 (2006) 65.
[11] J. Pola, D. Pokorná, M.J. Diánez, M.J. Sayagués, Z. Bastl, V. Vorlíček, Appl. Organomet. Chem. 19 (2005) 854.
[12] (a) R. Tomovska, V. Vorlíček, J. Boháček, J. Šubrt, J. Pola, New J. Chem. 29 (2005) 785;

(b) R. Tomovska, V. Vorlíček, J. Boháček, J. Šubrt, J. Pola, J. Photochem. Photobiol. A: Chem. 182 (2006) 107.
[13] J.J. Zhu, H. Wang, in: H.S. Nalwa (Ed.), Encyclopedia of Nanoscience and Nanotechnology, vol. 10, American Science Publishers, Steveson Ranch, 2004, p. 347.
[14] (a) -S.M. Lee, -Y.W. Jun, -S.N. Cho, J. Cheon, J. Am. Chem. Soc. 124 (2002) 11244;
(b) S. Chen, W. Liu, Mater. Chem. Phys. 98 (2006) 183;
(c) -S.Y. Hong, R. Popovitz-Biro, Y. Prior, R. Tenne, J. Am. Chem. Soc. 125 (2003) 10470;
(d) X.-L. Gou, J. Chen, P.-W. Shen, Mater. Chem. Phys. 93 (2005) 557.
[15] (a) J. Peters, B. Krebs, Acta Crystallogr. B38 (1982) 1270;
(b) M. Tenhover, R.S. Henderson, D. Lukco, M.A. Hazle, R.K. Grasselli, Solid State Commun. 51 (1984) 455;
(c) A. Pradel, V. Michel-Lledos, M. Ribes, Chem. Mater. 5 (1993) 377.
[16] (a) M. Tenhover, M.A. Hazle, R.K. Grasselli, Phys. Rev. 28B (1983) 4608;
(b) J.E. Griffiths, M. Malyj, G.P. Espinosa, J.P. Remeika, Phys. Rev. 30B (1984) 6978;
(c) D. Selvanathan, W.J. Bresser, P. Boolchand, Phys. Rev. 61B (2000) 15061.
[17] (a) J. Lebreton, G. Bosser, J. Ferran, L. Marsigny, J. Phys. B: At. Mol. Phys. 8 (1975) L141;
(b) E.G. Vago, R.F. Barrow, Proc. Phys. Soc. 58 (1946) 538;
(c) G. Lakshminaryana, B.J. Shetty, J. Mol. Spectrosc. 130 (1988) 155.
[18] L. Andrews, P. Hassanzadeh, D.V. Lanzisera, G.D. Brabson, J. Phys. Chem. 100 (1996) 16667.
[19] U.S. Dept. of Commerce, NIST, NIST X-ray Photoelectron Spectroscopy Database version 2, U.S. Dept. of Commerce, NIST, Gaithersburg, MD 20899, 1997.
[20] J.H. Scofield, J. Electron Spectrosc. Relat. Phenom. 8 (1976) 129.
[21] (a) H.S. Gutowsky, E.O. Stejskal, J. Chem. Phys. 22 (1954) 939;
(b) G.W. Bethke, M.K. Wilson, J. Chem. Phys. 26 (1957) 1107.
[22] J.R. Allkins, P.J. Hendra, Spectrochim. Acta 22 (1966) 2075.
[23] J.G. Martin, H.E. O'Neal, M.A. Ring, Int. J. Chem. Kinet. 22 (1990) 613.
[24] P.A. Longway, F.W. Lampe, J. Am. Chem. Soc. 103 (1981) 6813.
[25] (a) E. Golusda, K.-D. Lühmann, G. Mollekopf, M. Wacker and H. Stafast, E. C. 10th Eur. Photovoltaic Sol, Energy Conf., Proc. Int. Conf., 1991. p. 143;
(b) M. Frenklach, L. Ting, H. Wang, M.J. Rabinowitz, Israel J. Chem. 36 (1996) 293.
[26] D. Pokorná, M. Urbanová, Z. Bastl, J. Šubrt, J. Pola, J. Anal. Appl. Pyrolysis 71 (2004) 635.
[27] M. Santos, L. Díaz, M. Urbanová, D. Pokorná, Z. Bastl, J. Šubrt, J. Pola, J. Anal. Appl. Pyrolysis 76 (2006) 178.
[28] J.O. Chu, D.B. Beach, R.D. Estes, J.M. Jasinski, Chem. Phys. Lett. 143 (1988) 135.
[29] K. Sunanda, S. Gopal, B.J. Shetty, G. Lakshminarayana, J. Quant. Spectrosc. Radiat. Transfer 42 (1989) 631.
[30] W. Daily, Prog. Energy Combust. Sci. 23 (1997) 133.
[31] S. Chattopadhyaya, K. Kumar Das, Chem. Phys. Lett. 382 (2003) 249.
[32] O.W. Richardson, Molecular Hydrogen and Its Spectrum, Yale University Press, New Heaven, 1934.
[33] G.H. Dieke, J. Mol. Spectrosc. 2 (1958) 494.
[34] K.P. Huber, G. Herzberg, Molecular Spectra and Molecular Structure. Constants of Diatomic Molecules, Van Nostrand-Reinhold, New York, 1979.
[35] C.B. Winstead, S.J. Paukstis, J.L. Gole, J. Mol. Spectrosc. 173 (1995) 311.
[36] R.F. Barrow, G.G. Chandler, C.B. Meyer, Philos. Trans. R. Soc. London Ser. A 260 (1966) 395.
[37] F.W. Dalby, J. Vigué, J.C. Lehmann, Can. J. Phys. 53 (1975) 140.
[38] M. Castillejo, R. de Nalda, M. Oujda, L. Díaz, M. Santos, J. Photochem. Photobiol. A: Chem. 110 (1997) 107.
[39] J. Pola, M. Urbanová, L. Díaz, M. Santos, Z. Bastl, J. Subrt, J. Organomet. Chem. 605 (2000) 202.
[40] M. Santos, L. Díaz, J. Pola, J. Photochem. Photobiol. A: Chem. 152 (2002) 17.
[41] J.S. Francisco, J.I. Steinfeld, Spectrochim. Acta A 43 (1987) 207.
[42] J.W. Thoman Jr., J.I. Steinfeld, R.I. McKay, A.E.W. Knight, J. Chem. Phys. 86 (1987) 5909.
[43] G. Duxbury, A. Alijah, R.R. Trieling, J. Chem. Phys. 98 (1993) 811.
[44] M. Fukushima, S. Mayama, K. Obi, J. Chem Phys. 96 (1992) 44.
[45] E. Borsella, R. Antoni, Chem. Phys. Lett. 150 (1988) 542.
[46] M. Santos, L. Díaz, J.A. Torresano, J. Pola, J. Photochem. Photobiol. A: Chem. 104 (1997) 19.
[47] G. Bosser, J. Lebreton, L. Marsigny, J. Chim. Phys. 74 (1977) 13.
[48] J. Lebreton, G. Bosser, L. Marsigny, J. Phys. B 8 (1975) L141.
[49] T.J. Butennhoff, E.A. Rohlfing, J. Chem. Phys. 95 (1991) 3939.
[50] J.O. Odden, P.K. Egeberg, A. Kjekshus, J. Non-Cryst. Solids 14–15 (2005) 1317 (and refs. therein).
[51] Infrared Structural Correlation Tables and Data Cards, Heyden & Son Ltd., Spectrum House, London, Table 9, 1969.
[52] S. Al-Dallal, S. Aljishi, M. Hammam, S.M. Al-Alawi, M. Stutzmann, S. Jin, T. Muschik, R. Schwarz, J. Appl. Phys. 70 (1991) 4926.
[53] G. Lucovsky, in: E. Gerlach, P. Grosse (Eds.), The Physics of Selenium and Tellurium, Proc. Int. Conf. Königstein, Germany, Springer Verlag, Berlin, 1979, p. 178.
[54] P. Colomban, M.-P. Etcheverry, M. Asquier, M. Bounnichou, A. Tournié, J. Raman Spectrosc. 37 (2006) 614.
[55] E.A. Ebsworth, R. Taylor, L.A. Woodward, Trans. Faraday Soc. 55 (1959) 211.
[56] Z. Bastl, H. Bürger, R. Fajgar, D. Pokorná, J. Pola, M. Senzlober, J. Šubrt, M. Urbanová, Appl. Organomet. Chem. 10 (1996) 83.
[57] Z. Bastl, I. Spirovová, J. Horák, Solid State Ionics 95 (1997) 315.
[58] I. Ikemoto, K. Kikuchi, K. Yakuschi, H. Kuroda, Solid State Commun. 42 (1982) 257.
[59] H. Ogawa, T. Hattori, Appl. Phys. Lett. 61 (1972) 577.
[60] M.R. Alexander, R.D. Short, F.R. Jones, M. Stollenwerk, J. Zabold, W. Michaeli, J. Mater. Sci. 31 (1996) 1879.
[61] L. Brewer, K. Edwards, J. Phys. Chem. 58 (1954) 351.
[62] R.F. Porter, W.A. Chupka, M.G. Inghram, J. Chem. Phys. 23 (1955) 216.
[63] A. Songsasen, P.L. Timms, J. Mater. Chem. 10 (2000) 347.
[64] H.R. Philipp, J. Non-Cryst. Solids 8–10 (1972) 627.
[65] E. Füglein, U. Schubert, Chem. Mater. 11 (1999) 865.
[66] L. Andrews, P. Hassanzadeh, D.V. Lanzisera, G.D. Brabson, J. Phys. Chem. 100 (1996) 16673.
[67] J.E. Grifith, M. Malyj, G.P. Espinosa, J.P. Remeika, Phys. Rev. B 30 (1984) 6978.
[68] S. Chattopadhyaya, K.K. Das, Chem. Phys. Lett. 382 (2003) 249.
[69] E.T. Schaschel, D.N. Gray, P.L. Timms, J. Organomet. Chem. 35 (1972) 69.